U.R.S.I. FRANCE JS 26

INTELLIGENT TOOLS AND METHODS FOR RADIO SCIENCE

Physics-Informed Deep Learning for Efficient EMF Exposure Prediction

Shuangning Li[1], Yarui Zhang[2], Shanshan Wang[3], Joe Wiart[4]

[1]Chaire C2M, LTCI, Télécom Paris, Institut Polytechnique de Paris, shuangning.li@telecom-paris.fr
[2]SATIE Laboratory, Université Paris-Saclay, yarui.zhang@ens-paris-saclay.fr
[3]Chaire C2M, LTCI, Télécom Paris, Institut Polytechnique de Paris, shanshan.wang@telecom-paris.fr
[4]Chaire C2M, LTCI, Télécom Paris, Institut Polytechnique de Paris, joe.wiart@telecom-paris.fr

Keywords: EMF Exposure Prediction, Physics-Informed learning, Deep learning

Abstract

Accurate electromagnetic field (EMF) exposure mapping is essential for wireless network planning and digital twin communications. Existing deep learning methods typically formulate propagation estimation as a regression task without enforcing physical consistency. In this paper, we propose Phy-ExposNet, a two-stage framework that integrates a physics-informed estimation module with a transformer-based refinement module. The first stage reconstructs the electromagnetic field under physical constraints, while the second stage refines the exposure map by modeling long-range interactions and complex spatial patterns. Experimental results on benchmark datasets show that the proposed method achieves state-of-the-art performance, reducing prediction error by approximately 15% compared to strong baselines, while using over 80% fewer parameters than conventional physics-informed models.

1 Introduction

Electromagnetic field (EMF) exposure estimation plays a crucial role in modern wireless network planning, environmental monitoring, and digital twin communications [1], [2]. EMF exposure maps, closely related to radio maps, characterize the spatial distribution of signal or field intensity over a geographical area and support key applications such as coverage optimization, resource allocation, and compliance with safety regulations [3], [4]. In downlink scenarios, exposure levels are strongly correlated with received signal strength, making EMF exposure mapping closely connected to path loss estimation.

Despite extensive research, accurate and scalable EMF exposure mapping remains challenging. Traditional approaches include measurement-based methods and model-based prediction. While measurement campaigns provide reliable local characterization, they are costly and difficult to scale to large urban environments [5]. Empirical propagation models are computationally efficient but lack accuracy in complex scenarios, whereas ray-tracing methods achieve high fidelity at the expense of prohibitive computational cost [6]. These limitations motivate the development of efficient yet physically consistent learning based solutions.

Recent advances in deep learning have demonstrated strong potential for radio map estimation. CNN based models such as RadioUNet [7] and its extensions [8], [9] achieve near ray-tracing accuracy with significantly reduced computation. These approaches have also been extended to EMF exposure prediction [10]. However, most existing methods treat propagation estimation as a purely data-driven regression problem, without enforcing physical consistency, leading to poor generalization and unreliable predictions in complex environments.

Physics-informed machine learning has emerged as a promising direction to address this limitation. By embedding physical laws such as partial differential equations into the learning process, physics-informed neural networks (PINNs) provide improved generalization and interpretability [11]. In the electromagnetic domain, recent works incorporate the Helmholtz equation or volume integral equation (VIE) into neural networks to enforce physical constraints [12], [13]. For instance, PEFNet [14] integrates VIE-based loss into path loss prediction, demonstrating the effectiveness of combining data-driven learning with electromagnetic theory.

Nevertheless, most existing methods rely on convolutional architectures, which inherently capture only local spatial interactions. This limitation restricts their ability to model long-range propagation effects, such as diffraction and complex shadowing, which are essential for high-resolution EMF exposure mapping. Transformer architectures [15], with their global self-attention mechanism, provide a natural solution to this limitation by modeling long-range dependencies across the entire spatial domain.

In this paper, we propose Phy-ExposNet, a two-stage framework that integrates physics-informed field estimation with transformer-based refinement. The first stage reconstructs the electromagnetic field under physical constraints, capturing global propagation behaviour, while the second stage refines the exposure map by modelling long-range interactions and complex spatial patterns. Especially, the integration of complementary physical priors by jointly incorporating the volume integral equation (VIE) and partial differential equation (PDE) formulations of electromagnetic propagation. By constraining the network from both integral and differential perspectives, the model is encouraged to learn more physically consistent and expressive representations of electromagnetic field interactions, leading to improved prediction accuracy.

2 ELECTROMAGNETIC BACKGROUND AND THEORETICAL FORMULATIONS

This section summarizes the electromagnetic principles underlying the proposed physics-informed framework. We briefly introduce the frequency-domain formulation, the Helmholtz equation, and the volume integral equation (VIE), which together provide complementary local and global physical constraints for training.

2.1 Maxwell's Equations in the Frequency Domain

Under time-harmonic excitation, electromagnetic fields can be described in the frequency domain by Maxwell's equations:

$$\nabla \times \boldsymbol{E} = -j\omega \boldsymbol{B} \quad , \nabla \times \boldsymbol{H} = \boldsymbol{J} + j\omega \boldsymbol{D} \tag{1}$$

For linear isotropic media, the material response is given by:

$$D = \varepsilon E, \quad , B = \mu H, \quad , J = \sigma E \tag{2}$$

To unify dielectric and conductive effects, the complex permittivity is defined as:

$$\varepsilon_c = \varepsilon_0 \varepsilon_r - j\frac{\sigma}{\omega} \tag{3}$$

2.2 Helmholtz Equation and PDE Constraint

By eliminating the magnetic field, Maxwell's equations can be reduced to a wave equation in terms of the electric field:

$$\nabla \times \nabla \times E - \omega^2 \mu \varepsilon_c E = 0 \tag{4}$$

Under the assumption of negligible charge accumulation, this leads to the Helmholtz equation:

$$\nabla^2 E + k^2 E = 0 \tag{5}$$

Where $k^2 = \omega^2 \mu\, \varepsilon_c$, In practice, since the exact medium properties are unknown, we adopt a relaxed formulation:

$$\nabla^2 E^{tot} + \beta E^{tot} = 0 \tag{6}$$

Based on this, the PDE residual loss is defined as:

$$L_{PDE} = \frac{1}{N}\sum |\nabla^2 \hat{E} - \beta \hat{E}|^2 \tag{7}$$

This term enforces local physical consistency of wave propagation.

2.3 Volume Integral Equation (VIE) and Global Constraint

To model global scattering effects, we adopt the volume integral equation. For the 2-D transverse magnetic case, the total field satisfies:

$$E^{\mathrm{tot}}(p) = E^{\mathrm{inc}}(p) + k_0^2 \int_D G(p - p')\chi(p')E^{\mathrm{tot}}(p')dp' \tag{8}$$

After discretization, this can be written in matrix form:

$$(I + W\chi)E^{tot} = E^{inc} \tag{9}$$

The corresponding VIE residual loss is:

$$L_{VIE} = \frac{1}{N}|(I + W\chi)\hat{E} - E^{inc}|_2^2 \tag{10}$$

This term enforces global consistency by modeling interactions between all scattering elements.

2.4 Physics-Guided Loss Design

Finally, the PDE and VIE constraints are combined:

$$L_{phys} = \lambda_{PDE}L_{PDE} + \lambda_{VIE}L_{VIE} \tag{11}$$

The overall training objective is:

$$L = L_{data} + L_{phys} \tag{12}$$

The PDE term captures local propagation behavior, while the VIE term models global scattering interactions. Their combination provides complementary physical constraints, enabling the network to learn more accurate and physically consistent electromagnetic field representations.

3 Phy-ExposNet ARCHITECTURE

This section presents the overall architecture of the proposed framework. The model follows a two-stage design consisting of a physics-guided field estimation stage and an attention-based residual refinement stage. The first stage produces a physically meaningful electromagnetic field representation, while the second stage improves prediction accuracy through residual correction.

3.1 Stage 1: Physics-Guided Field Estimation

The input to the network consists of four components: a building mask, a transmitter location mask, and the real and imaginary parts of the incident electromagnetic field. The building mask encodes the spatial distribution of obstacles, while the transmitter mask indicates the source location. The incident field provides an explicit physical prior, enabling the network to focus on learning the scattering effects introduced by the environment.

Based on these inputs, the first-stage network predicts the complex total electromagnetic field. This mapping is implemented using a lightweight encoder–decoder architecture with skip connections, allowing the model to capture both large-scale propagation behaviors, such as diffraction and shadowing, and finer spatial details.

An initial path loss map is then derived from the predicted field through a magnitude-to-logarithmic transformation. This stage provides a physically consistent coarse estimate that serves as the foundation for subsequent refinement.

3.2 Stage 2: Attention-Based Residual Refinement

To further improve accuracy, a refinement module is introduced to learn the residual error between the initial estimate and the ground truth. The final prediction is obtained by adding this residual correction to the initial path loss map.

The refinement network adopts an attention-enhanced encoder–decoder structure. Instead of conventional spatial self-attention, a channel-oriented attention mechanism is employed to capture inter-channel dependencies with lower computational complexity. This design enables efficient global information exchange while preserving local spatial structures.

In addition, a gated depthwise feed-forward mechanism is used to enhance feature representation. By adaptively modulating feature responses, this module improves the modeling of complex propagation effects, particularly in challenging regions such as building boundaries and shadow transitions.

By focusing on residual learning, the refinement stage reduces optimization difficulty and enhances training stability.

3.3 Overall Framework

The overall framework can be viewed as a composition of the two stages as shown in Figure 1. The first stage produces a physics-guided coarse estimate of the propagation field, while the second stage refines this estimate by modeling complex interactions that are difficult to capture using physical priors alone.

This decomposition separates global structure modeling from local error correction, leading to improved interpretability and performance. As a result, the proposed framework achieves a strong balance between physical consistency, prediction accuracy, and computational efficiency.

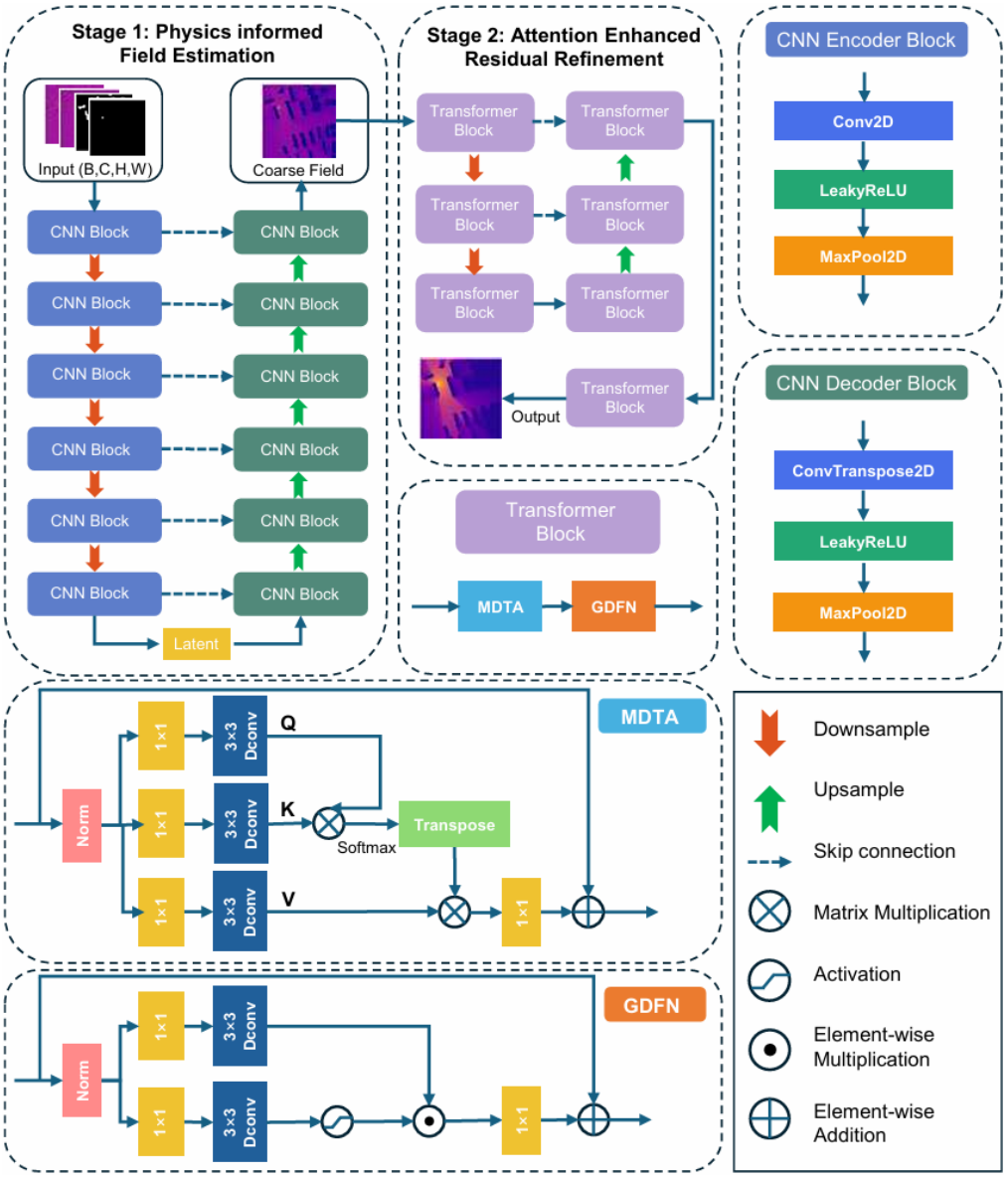

Figure 1: Overview of the proposed two stage architecture for EMF exposure prediction

4 Simulation and results

4.1 Dataset

We evaluate the proposed Phy-ExposNet on two representative datasets, namely RadioMapSeer and a measurement-driven dataset derived from PMNet referred to as USC-PL.

RadioMapSeer is a large-scale simulated dataset for urban path loss prediction, consisting of 700 scenarios with 80 transmitter locations each (56,000 samples in total). The data are generated at 5.9,GHz on a 256 × 256 grid with 1 m resolution, using building layouts from OpenStreetMap and the Dominant Path Model (DPM). Each sample includes a building mask, a transmitter mask, and the corresponding path loss map.

USC-PL is a measurement-driven dataset collected at 2.5 GHz, reflecting realistic propagation conditions with environmental uncertainty. The original maps are cropped into 221 × 221 patches with a resolution of approximately 0.86 m, resulting in 4754 samples. Compared to simulation-based data, USC-PL provides a more challenging benchmark for evaluating model robustness and generalization. For both datasets, we adopt the standard train, validation and test splits used in prior works to ensure fair comparison.

4.2 Implementation Details

All models are implemented in PyTorch and trained on NVIDIA A100 GPUs. The training is conducted for 50 epochs with a batch size of 16.

The physics loss weights are set to 0.5 ensuring balanced contributions from the two physical constraints. The PDE parameter β is set to 0.1. This configuration allows the model to jointly leverage physics-based regularization and supervised learning signals for stable training and improved generalization.

4.3 Evaluation Metrics

We evaluate performance using four metrics: NMSE, RMSE, MAE, and SSIM, which jointly assess numerical accuracy and structural consistency.

- NMSE measures relative reconstruction error and is reported in dB.
- RMSE reflects average prediction error and is sensitive to large deviations.
- MAE provides a robust measure of average absolute error.
- SSIM evaluates structural similarity, reflecting how well spatial propagation patterns are preserved.

Together, these metrics provide a comprehensive evaluation of both global accuracy and spatial fidelity.

4.4 Numerical Results

Figure 2 shows a qualitative comparison of different methods. Empirical models like ITU-R and 3GPP fail to capture environment dependent propagation effects and produce overly smooth results. Classical machine learning methods XGBoost and KNN improve slightly but suffer from spatial inconsistency and blurred structures.

Deep learning models, including RadioUNet and PEFNet, capture global attenuation trends but still exhibit over-smoothing and inaccuracies in shadow regions. In contrast, the proposed Phy-ExposNet produces predictions that closely match the ground truth, accurately preserving shadow boundaries, directional propagation, and spatial structures.

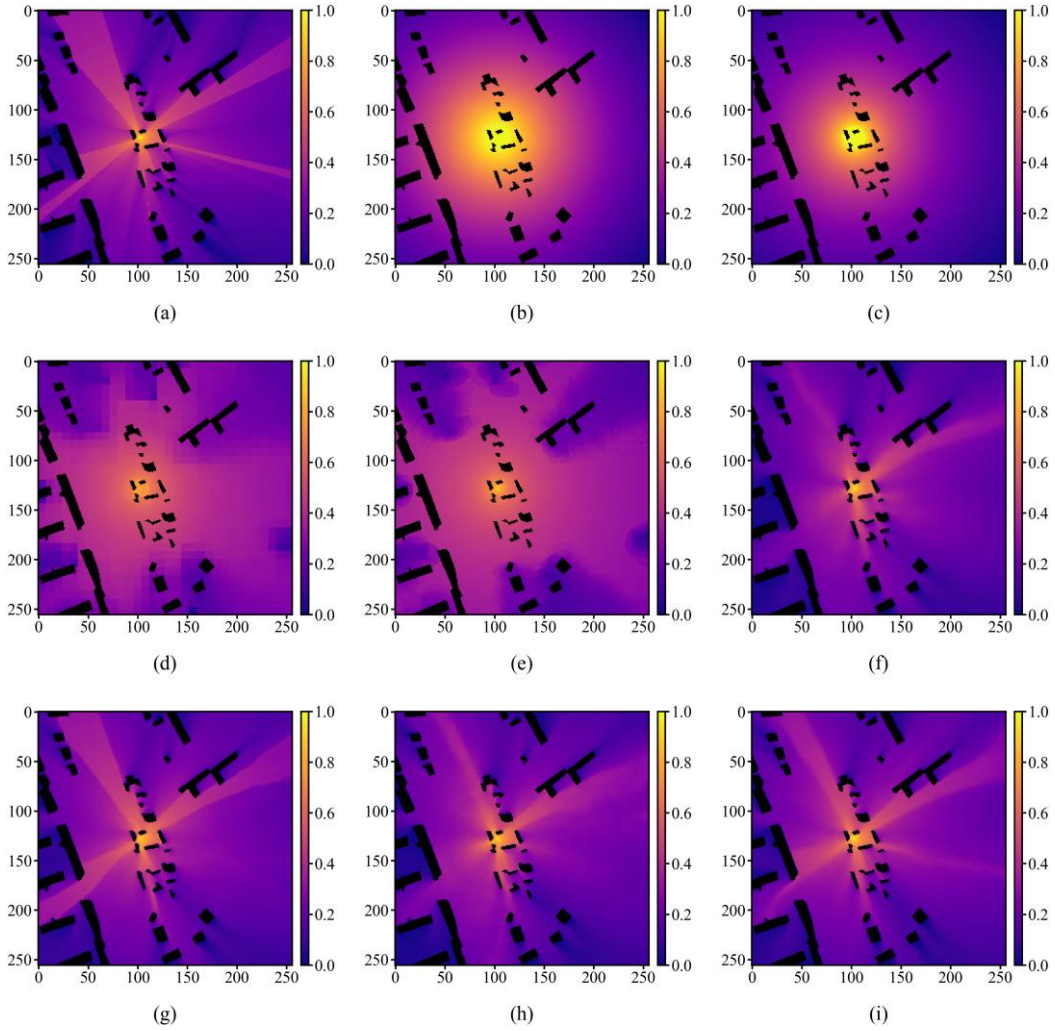

Figure 2: Visualization comparison of different methods on the RadioMapSeer dataset.From (a) to (i): (a) ground truth, (b) ITU-R IMT-2020, (c)

3GPP38.901, (d) XGBoost, (e) KNN, (f) RadioUnet, (g) PEFNet, (h) ResNet, (i) Phy-ExposNet

Table 1 reports the quantitative comparison on two datasets. It can be observed that empirical models (ITU-R IMT-2020 and 3GPP38.901) and classical machine learning methods (XGBoost and KNN) consistently yield significantly inferior performance across all metrics. Their NMSE and RMSE remain high, and the SSIM values indicate poor reconstruction of spatial propagation structures, suggesting that these approaches are unable to capture complex environment-dependent propagation effects.

Table 1: Performance comparison on two datasets

Method	**RadioMapSeer**				**USC-PL**			
	NMSE (dB)	**RMSE**	**MAE**	**SSIM**	**NMSE (dB)**	**RMSE**	**MAE**	**SSIM**
ITU-R IMT-2020	0.88	0.2001	0.1469	0.5277	-4.92	0.3743	0.3069	0.6089
3GPP38.901	-2.51	0.1355	0.0968	0.5789	-3.57	0.4376	0.3715	0.5072
XGBoost	-1.16	0.1559	0.1217	0.4601	-15.74	0.1046	0.0802	0.7960
KNN	-0.87	0.1624	0.1183	0.5106	-14.57	0.1182	0.0834	0.8592
RadioUnet	-18.49	0.0230	0.0120	0.9022	-25.81	0.0324	0.0217	0.9261
PEFNet	-17.89	0.0239	0.0129	0.9006	-28.08	0.0235	0.0157	0.9304
ResNet	-18.78	0.0221	0.0124	0.8992	-28.27	0.0236	0.0155	0.9378
Phy-ExposNet	**-19.87**	**0.0195**	**0.0102**	**0.9194**	**-30.79**	**0.0173**	**0.0112**	**0.9540**

We therefore focus on the comparison with deep learning based methods. On RadioMapSeer, all neural models achieve competitive results, but Phy-ExposNet consistently outperforms existing methods. Compared with ResNet, it reduces RMSE by approximately 12% and MAE by 18%, while improving SSIM, indicating better accuracy and structural preservation.

On the more challenging USC-PL dataset, performance differences become more pronounced. While baseline models show increased errors, Phy-ExposNet remains stable and achieves the best performance across all metrics, with approximately 14% RMSE improvement over RadioUNet.

Furthermore, to validate the necessity of the proposed two stage architecture and the incorporation of physics informed losses, we conduct an ablation study by comparing different model configurations. Specifically, we consider three variants:

(i) a two stage network trained without physics informed losses,

(ii) a single stage refinement network trained only with supervised MSE loss, and

(iii) the proposed Phy-ExposNet. The predictions are further compared with the ground truth.

Figure 3 presents qualitative results on two test samples. It can be observed that the single stage refinement model, although capable of capturing the overall signal distribution, tends to produce overly smooth predictions and fails to accurately reconstruct electromagnetic spatial variations. Similarly, the two stage model without physics informed constraints improves the global structure but still exhibits noticeable deviations in complex propagation regions.

In contrast, the proposed Phy-ExposNet achieves predictions that are visually the closest to the ground truth. In particular, as highlighted in the red boxed regions, the proposed model better captures detailed electromagnetic propagation patterns such as shadowing effects, reflection, and directional signal attenuation. These results indicate that the integration of physics informed losses effectively guides the model toward physically consistent solutions.

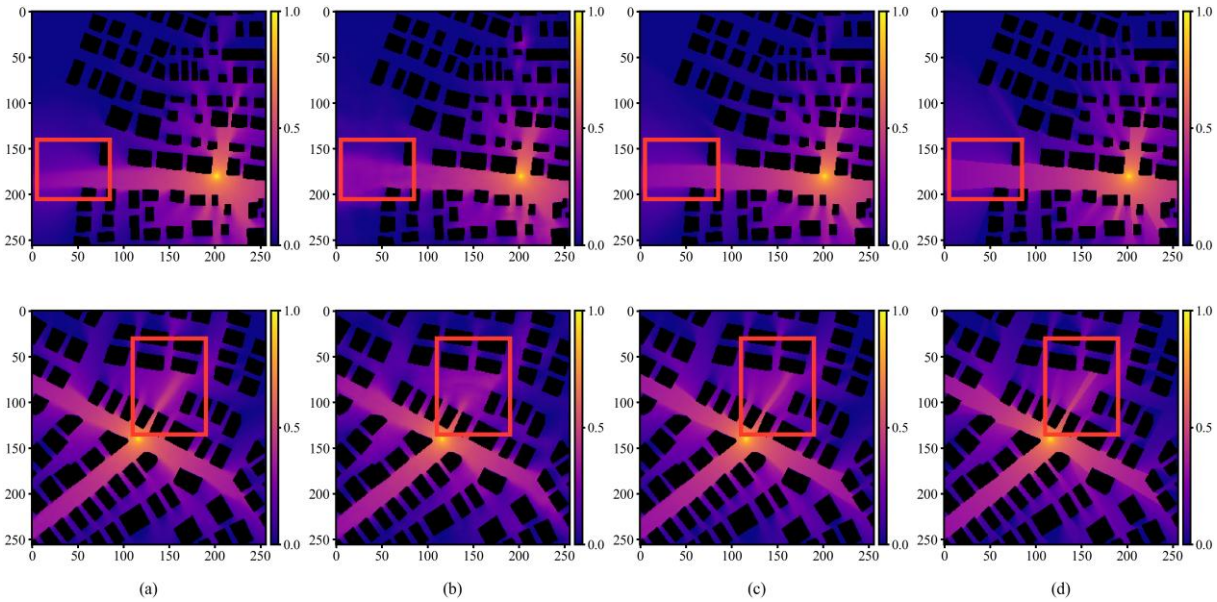

Figure 3: Comparison of ablation models on two test samples. From (a) to (d): (a) Two stage model without physical loss, (b) Only stage2 model, (c) Phy-ExposNet, (d) Ground Truth

5 Conclusion

In this paper, we have presented Phy-ExposNet, a physics informed two stage transformer refinement network for accurate exposure mapping estimation. The key insight motivating our design is that exposure mapping estimation benefits from a clean separation between coarse propagation structure estimation and residual correction, with each stage optimized for its specific role.

Several directions remain open for future work. First, extending Phy-ExposNet to 3-D environments and higher frequencies is a natural next step.Second, improving the VIE loss computation for lossy building materials could further tighten the physics constraints in realistic scenarios. Third, incorporating antenna pattern information and beamforming configurations as additional input features may extend the framework's applicability to massive MIMO network planning. Finally, data efficient transfer learning strategies built on the physics informed representation learned by network could reduce the labeled data requirements for new deployment scenarios.

Acknowledgements

This work benefited from a government grant managed by ANR agency under the France 2030 program, reference ANR-22-PEFT-0008.

References

[1] S. Faye *et al.*, “A Survey on EMF-Aware Mobile Network Planning,” *IEEE Access*, vol. 11, pp. 84568–84597, 2023.

[2] S. Tadik *et al.*, “Digital Spectrum Twins for Enhanced Spectrum Sharing and Other Radio Applications,” *IEEE J. Radio Freq. Identif.*, 2024.

[3] X. Liu *et al.*, “Channel Knowledge Maps for 6G Wireless Networks: Construction, Applications, and Future Challenges,” *arXiv preprint arXiv:2505.24151*, 2025.

[4] ICNIRP, “Guidelines for Limiting Exposure to Electromagnetic Fields (100 kHz to 300 GHz),” *Health Physics*, vol. 118, no. 5, pp. 483–524, 2020.

[5] J. Guillén-Pina *et al.*, “Efficient Design of Electromagnetic Field Exposure Maps with Multi-Method Evolutionary Ensembles,” *Environmental Research*, vol. 278, p. 121636, 2025.

[6] Y. Luo, J. Zhang, and P. Tang, “Survey of Indoor Radio Propagation Channel Measurements and Modeling,” *IEEE Access*, vol. 9, pp. 19622–19643, 2021.

[7] R. Levie *et al.*, “RadioUNet: Fast Radio Map Estimation With Convolutional Neural Networks,” *IEEE Trans. Wireless Commun.*, vol. 20, no. 6, pp. 4001–4015, Jun. 2021.

[8] Z. Yi *et al.*, “Feature Extraction in Reference Signal Received Power Prediction Based on Convolution Neural Networks,” *IEEE Commun. Lett.*, vol. 25, no. 6, pp. 1751–1755, Jun. 2021.

[9] Y. Zheng *et al.*, “Cell-Level RSRP Estimation With the Image-to-Image Wireless Propagation Model Based on Measured Data,” *IEEE Trans. Cogn. Commun. Netw.*, vol. 9, no. 6, pp. 1412–1425, Dec. 2023.

[10] A. Saeizadeh *et al.*, “AIRMap: AI-Generated Radio Maps for Wireless Digital Twins,” *arXiv preprint*, 2025.

[11] Y. Zhang, S. Wang, and J. Wiart, “ExposNet: A Deep Learning Framework for EMF Exposure Prediction in Complex Urban Environments,” *arXiv preprint arXiv:2503.02966*, 2025.

[12] M. Raissi, P. Perdikaris, and G. E. Karniadakis, “Physics-Informed Neural Networks: A Deep Learning Framework for Solving Forward and Inverse Problems Involving Nonlinear Partial Differential Equations,” *J. Comput. Phys.*, vol. 378, pp. 686–707, 2019.

[13] M. Nohra and S. Dufour, “Approximating Electromagnetic Fields in Discontinuous Media Using a Single Physics-Informed Neural Network,” *arXiv preprint arXiv:2407.20833*, 2024.

[14] R. Guo *et al.*, “Physics Embedded Deep Neural Network for Solving Volume Integral Equation: 2-D Case,” *IEEE Trans. Antennas Propag.*, vol. 70, no. 8, pp. 6135–6147, Aug. 2022.

[15] F. Jiang *et al.*, “Physics-Informed Neural Networks for Path Loss Estimation by Solving Electromagnetic Integral Equations,” *IEEE Trans. Wireless Commun.*, vol. 23, no. 10, pp. 15380–15394, Oct. 2024.